River Flow 2012 – Murillo (Ed.)
© 2012 Taylor & Francis Group, London, ISBN 978-0-415-62129-8

Automatic object detection to analyze the geometry of gravel grains – a free stand-alone tool

M. Detert & V. Weitbrecht
Laboratory of Hydraulics, Hydrology and Glaciology VAW, ETH Zurich, Switzerland

ABSTRACT: An automated procedure to estimate the grain size distribution of a gravel bed by analyzing its digital top-view photograph is presented. The MATLAB-based methodology allows for improved element separation compared with other approaches, including a Graphical User Interface for additional semi-automatic control and optional correction of the detected elements. First comparisons of grading curves obtained by automatic object detection, in-situ line sampling and laboratory sieving indicate a good agreement concerning the essential geometric parameters. The temporal effort for the automatic object detection is only a fraction of the time required using common methods. A further benefit is that additional parameters are provided for each grain as well, namely axis ratio, area, perimeter, center coordinates, and the horizontal grain orientation. Free access is given to the newly developed license-free stand-alone tool including the compiled code.

1 INTRODUCTION

The knowledge on the build-up of a river bed is essential for understanding and prediction of fluvial processes. For non-cohesive bed material, especially the grading curve and its characteristic grain sizes provide decisive parameters for modeling hydraulics and sediment transport. For instance, d_m is a fraction-weighted mean diameter and d_{90} gives the mass-percentile at 90% sieve throughput. However, the grain size distribution is important for additional aspects as well, e.g. to classify aquatic habitats or to evaluate geological deposits.

Common laboratory sieving requires a demanding effort on technique and personnel to classify sediments, while the whole process of digging, transport and sieving is time-consuming and cost-intensive. Alternatively, numerous in-situ methods were developed to gain grading curves, e.g. based on inventorying single grains by means of a grid (Wolman, 1954) or along a line (Fehr, 1987). Yet these methods are time-consuming as well, often insufficient in accuracy and hardly applied for a completely wetted bed.

Several automatic approaches were developed in recent years to analyze areal digital information from digital photography or laser scanning with a focus to achieve only one single characteristic grain size parameter. Successful procedures originate from Carbonneau et al. (2004, texture analysis of air-borne photographs), Heritage and Milan (2009, texture analysis of terrestrial laser-scanning), or Buscombe et al. (2010, frequency analysis of digital microphotographs).

Beyond this, techniques to detect and measure single grain areas in digital photographs allow for classifying the grain sizes at the uppermost layer of a gravel bed. Weichert et al. (2004) used a simple grayscale threshold approach to determine a binary image where single grain elements are separated from interstices. Graham et al. (2005a, 2005b) applied a double threshold approach based on identifying first the interstices by a grayscale threshold and then combining them with possible interstices determined with a bottom-hat filter (compare §2.1 and §2.2). The final separation of the grain elements results from a simple watershed algorithm (§2.4).

The work of Graham and co-workers is a significant step in the automation of grain size classification. However, there are several possibilities to optimize their procedure by: (a) preprocessing, omitting crude image filters; (b) detection of interstices by expanding the exclusive use of two image filters to the application of further filters; (c) improving the watershed algorithm, as it leads to over-segmentation and cannot be switched off; (d) handle of single grain elements within a post-processing by a Graphical User Interface (GUI); (e) statements concerning the non-detected fines. Prognosis approaches to estimate a grading curve of the subsurface layer lack (e.g. Fehr 1987); and (f) deriving a volumetric grading curve as obtained by classical sieving from a number per area grading curve as gained by object detection. Consequently, the possibility to transfer the results to classical approaches in hydraulics or sediment transport is limited.

Below an optimized object detection approach is developed that is inspired by the method of Graham and co-workers. First, the procedure to detect the interstices between the single grain elements within a grayscale image is described. Then, the grain areas are measured. In doing so, Graham's procedure is

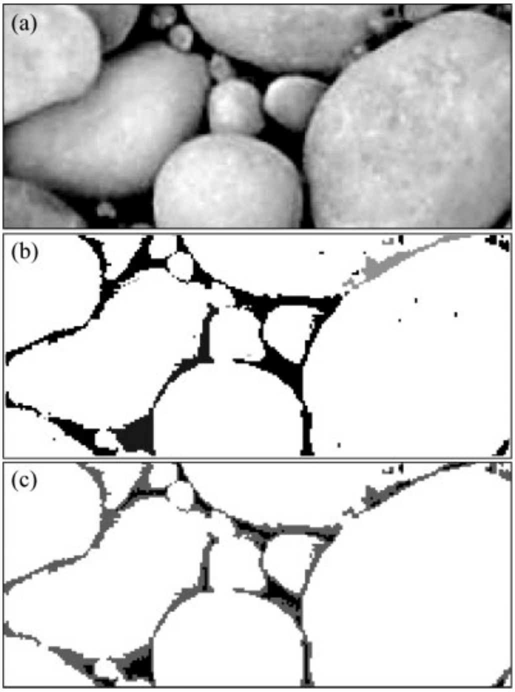

Figure 1. Double grayscale threshold (as cutout from Fig. 7). (a) Initial grayscale image, (b) Possible extended grayscale interstices estimated via 90% of Otsu's threshold. Different gray shading relates to individual objects in 8-connected neighborhood, (c) black: Definite grayscale interstices, determined via 50% of Otsu's threshold; gray: Confirmed extended grayscale interstices.

optimized in relation to items (a) to (d). Concerning items (e) and (f), the present GUI allows for analyzing the results from object detection following Fehr's (1987) approach to transfer surface information into a grain size distribution of the surface and subsurface material. The applied algorithms for image processing are implemented in MATLAB toolboxes (MATLAB, 2012).

2 OBJECT DETECTION

2.1 *Step 1: Interstice detection by double grayscale threshold*

Within the first step interstices are detected using a double grayscale threshold approach (Fig. 1a-c).

A top view photograph of a granular bed is converted to a grayscale image (Fig. 1a) to apply Otsu's gray-thresh function (MATLAB, 2012). This method minimizes the intra-class variance of the pixels. Single threshold values in an 8×8 px^2 block structure were determined. To avoid sharp edges, the resulting threshold matrix is smoothed afterwards by a median-filter in a neighborhood of 16×16 px^2. Possible interstices are determined in a binary image of the grayscale photograph with a threshold level of 90% of Otsu's

Figure 2. Bottom-hat operations. (a) possible interstices estimated by binary image of bottom-hat filtered grayscale image. Different gray shading relates to individual object determined in a 4-connected neighborhood, (b) black: interstices confirmed by extended grayscale interstices; gray: confirmed definite grayscale interstices.

smoothed threshold matrix. To suppress intra-granular noise a small median-filter of 3×3 px^{2}or 5×5 px^2 can be applied optionally to the photograph. Individual interstice areas are object-detected in an 8-connected neighborhood (Fig. 1b). These areas are feature-AND operated by smaller 'islands' of definite interstices in a binary image with a threshold level of 50% of Otsu's threshold matrix, i.e. possible interstices are confirmed if they are connected to definite interstices (Fig. 1c).

The result of step 1 is one matrix with definite grayscale interstices (black areas, Fig. 1c), and another matrix with confirmed extended grayscale interstices (gray areas, Fig. 1c). The latter is used within feature-AND operations in the next steps.

2.2 *Step 2: Interstice detection by morphological bottom-hat transform*

The second step applies a bottom-hat transformation technique to determine further interstices. A morphological bottom-hat filtering (MATLAB, 2012) is performed on the grayscale image (Fig. 1a) by a flat, disk-shaped structuring element of radius 1 px. The suppression of intra-granular noise radii up to 3 px is possible; a small median-filter of 3×3 px^{2}or 5×5 px^2 can be pre-applied alternatively to the grayscale photograph. The values of the resulting matrix are converted from numerical to logical data. Then, possible interstice areas are object-detected in a 4-connected neighborhood (Fig. 2a). These areas become feature-AND operated (Fig. 2b): Possible interstices are confirmed if they are connected by $\geq$5% of their area to confirmed extended interstices from step 1 (Fig. 1c).

At the end of step 2 the confirmed interstices from the first two steps are smoothed by a morphological

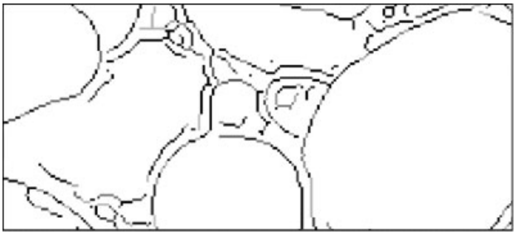

Figure 3. Canny edges: each gray shading relates to an individual edge as determined in a 4-connected neighborhood.

closing, i.e. dilation followed by erosion, performed by a flat, disk-shaped structuring element. Typically, the smallest possible radius of 1 px gives sufficient results for the next steps.

2.3 *Step 3: Interstice detection by edge detection methods*

The third step uses information of two gradient filter techniques, the Canny (Fig. 3) and the Sobel methods (MATLAB, 2012). However, other edge detection methods are applicable as well.

The Canny method finds edges by looking for local maxima of the derivative of a Gaussian filter of the grayscale photograph. The method uses two thresholds, to detect strong and weak edges, and includes the weak edges in the output only if they are connected to strong edges. This method is therefore less likely than other gradient filter to be misled by noise, and more likely to detect true weak edges. Possible interstice areas are object-detected in a 4-connected neighborhood (Fig. 3). These areas become feature-AND operated with the results from step 2 (Fig. 2b). At optimum conditions $\geq 25\%$ of their area must be congruent to confirmed extended interstices, and their area must be >2 px. However, slight changes of these values indicate only a slight effect onto the following processes.

The Sobel method simply finds edges using the Sobel approximation to the derivative of the grayscale image of the granular bed. The Sobel edges are used to feature-AND operate the Canny edges in the same way and based on the same criteria as for the confirmed extended interstices.

At the end of step 3 the confirmed interstices are smoothed by morphological operations.

2.4 *Step 4: Separation by watershed transform*

Within the fourth step the focus changes from detection of interstices to separation of single grain areas. This is done by the combination of Canny edges object-detected in an 8-connected neighborhood and by watershed bridges (Fig. 4). In the following, six parameters are chosen to steer the watershed separation process. The optimum ranges were found by empiricism, as presented below.

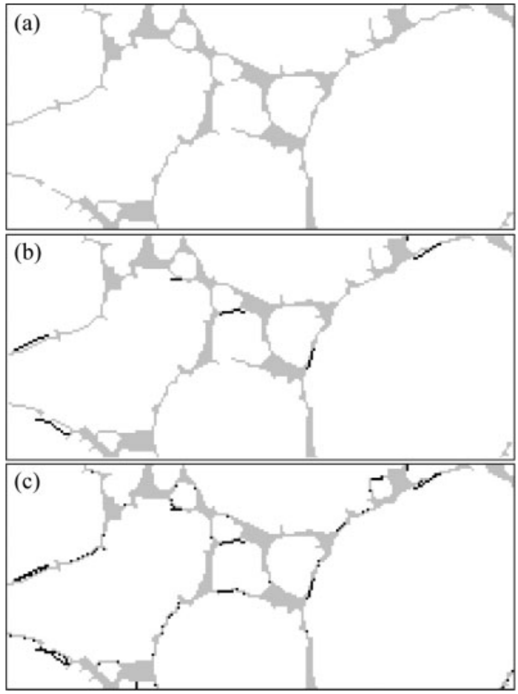

Figure 4. Watershed separation (a) initial binary image, (b) image-operated Canny bridges, confirmed by watershed bridges, (c) final separation, including Canny and watershed bridges.

To start the separation, the inverted binary outcome matrix of the previous step is operated by object-detection techniques in a 4-connected neighborhood to get the grain areas that were separated so far, thereby excluding elements with <25 px. The result is an initial binary image for the watershed operations (Fig. 4a). To determine single watershed regions, the H-minima transform is computed from the Euclidean distance transform of the initial binary image (MATLAB 2012). Watershed bridges now are found by the morphological difference between the initial binary image and the binary image of the watershed regions. To successfully separate the different grain regions a two-step separation procedure was applied as follows:

In the first separation step, the Canny edges of the initial binary image are feature-AND operated by watershed bridges of the same image matrix (Fig. 4b). The watershed bridges are dilated by a structuring disk-shaped element of radius 4 px to improve the procedure. Areas of Canny edges are confirmed if they are completely masked by the watershed bridges and if their interrelated orientation angle differs by $<10°$. Further, the ratio of length to breadth of the edges has to be >2 and their area has to be >3 px.

In the second separation step, watershed bridges are determined for the binary image of actual outcome from step 1. To suppress over-segmentation of larger grains, watershed bridges are confirmed if their area is >40 px.

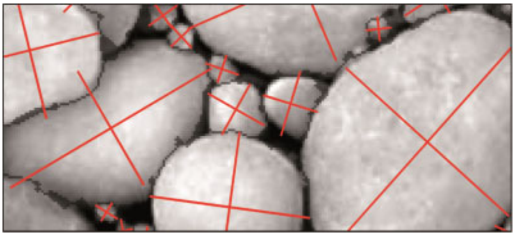

Figure 5. Final result of object detection procedure. Straight lines (colorprint: red) represent a-axis and b-axis of ellipses fitted to object areas using normalized second central moments of determined object areas.

The outcome of step 4 is a binary image with fully-confirmed single grain elements successfully separated by their interstices.

2.5 *Step 5: Final operations*

Step 5 is needed for final operations with the goal to obtain the region properties of each grains top view area. Smaller grains that were excluded in step 4 are included again. However, experience indicated so far, that grains areas < ∼20 px are hardly to detect at all, as confirmed by Graham et al. (2005b), who found a limit of 23 px. Boundary grains that are not fully included within the analyzed frame are blanked out, to avoid a misleading statistical analysis of the characteristic diameter. Optionally, a morphological smoothing of the detected grain elements is applied.

In the final step the areas are replaced with ellipses of the same normalized second central moments. Fig. 5 shows the axis of the replaced ellipses. The straight lines show the a-axis and b-axis, respectively. Additional parameters can be provided for each grain as well, e.g. the ratio a/b, area, perimeter, center coordinates, and the grain orientation in the horizontal plane. These can be used to further analyze the characteristics of the bed material with respect to bed roughness, or armoring processes, for instance.

3 TRANSFER TO A QUASI-SIEVE ANALYSIS

3.1 *Line-sampling analysis*

The line-sampling method is a user-friendly in-situ sampling method to analyze a gravel surface and to determine grain size distributions of the surface and subsurface bed material. Complex utilities are not needed. In short, the method is described as follows (Fehr, 1987): With a string or a measuring tape a line is spanned over an (at least almost) dry gravel bed. The b-axes of all grains are measured that are in contact to the line and that are larger than a threshold value of typically 10 mm (Fig. 6).

The sampling data are classified into fractions already in the sampling log. To ensure the representativeness of the analysis, at least 150 grains should

Figure 6. Line-sampling: Sketch, top-view. For subsequent analysis, b-axis of gray-shaded stones are measured if they contact the line.

be counted, while at least 30 grains of them should belong to medium grain-size fractions. The transfer calculation of a line-sampling of a surface layer to an equivalent grading curve of the subsurface layer comprises two steps; only then a comparison between line-sampling and volume-sampling is possible:

Within the first step, the distribution as 'number along a line' is transferred to a distribution as 'mass fraction per total mass', i.e. a quasi-sieve throughput, by

$$\Delta p_i = \frac{\Delta q_i \, d_{mi}^{0.8}}{\sum_1^n \Delta q_i \, d_{mi}^{0.8}} \tag{1}$$

with Δp_i = (weight of fraction i)/(weight of entire sample, Δq_i = (number of stones in fraction i)/(number of stones in entire probe), d_{mi} = characteristic (mean) grain-diameter of fraction i, n = number of fractions.

As grains < 10 mm are neglected within the sampling process, the cumulative frequency for the fines has to be corrected in a second step. Derived from an extensive data set, Fehr (1987) demonstrated that 20–30% of the subsurface layer volume in gravel bed rivers is < 10 mm in diameter. Thus, p_i has to be corrected toward p_{iC} via

$$p_{iC} = 0.25 + 0.75 \sum_1^i \Delta p_i \tag{2}$$

For a more precise depiction of the a priori estimation of a fraction of 25% fines, Fehr (1987) suggests an approximation by a Fuller distribution. Optionally, a flexible adaption to the fix estimated fraction of 25% fines is made by determining the overlap area of grading curve and the Fuller curve by a least-squares fit of their inclination.

3.2 *Digital image analysis*

Fig. 7 shows an example of a top-view photograph of a granular bed with 755 detected single grain areas according to the object detection involving steps 1–5, complemented by the lines to apply a line-sampling according to Fehr's (1987) method. The distance between the lines was a priori estimated to represent the characteristic mean grain diameter a (here: 100 px). All the objects in connection with the 17 lines in the x- and z-directions are analyzed following Fehr's method, leading finally to a grading curve and the characteristic grain diameters. Note that the pre-processing

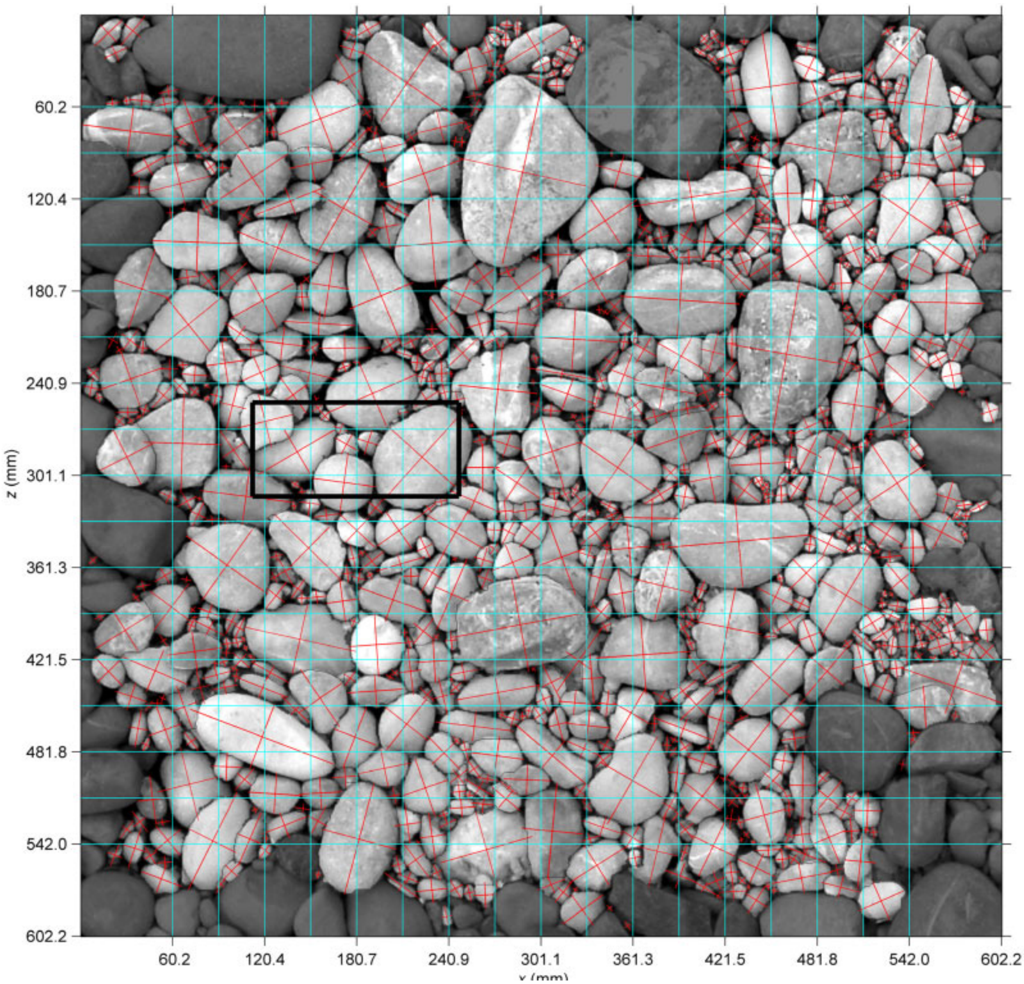

Figure 7. Detected and GUI-operated single grain areas within top-view photograph, scaling: 0.6022 mm/px. Light (colorprint: cyan) raster: lines apply to Fehr's (1987) method. Rectangular black box: cutout of Figs. 1–5. Further legend: see Fig. 5.

(image import, scaling, parameter selection and object detection) as well as the post-processing (cosmetic merging, departing, and exclusion of grains) resulting in Fig. 7 is handled by a GUI. Furthermore, the intermediate and final results can optionally be exported to common formats of Excel, comma-separated values or simple ASCII-text as well as in common image formats.

Fig. 8 shows the estimated grading curve of the subsurface material as a typical result of the detected and GUI-operated single grain areas from Fig. 7, compared with the results of an original in-situ line sampling and a classical sieve analysis conducted for the bed material at the same location. Overall, the grading curves match reasonably well. Apart from d_{30}, the resulting d_m and d_{90} differ only by <5% in the current example. A systematic analysis concerning the reliability of the present method as well as their limits of application is currently in preparation.

4 SUMMARY AND OUTLOOK

Inspired by approaches developed e.g. by Weichert et al. (2004) or Graham (2005a, 2005b) an automated non-destructive and contactless procedure is presented to estimate the grain size distributions of a granular river bed and its subsurface layer. The core of the methodology involves MATLAB-based object detection techniques applied to analyze digital top-view photographs of gravel layer surfaces. Compared with the approach of Graham and co-workers the present results are more accurate especially in the separation of the different area elements referring to top view areas of single grains. Each detected grain area is replaced with ellipses of the same normalized second central moments. Following Fehr's approach the line sampling is used to transfer the statistics of the *b*-axes into a quasi-grain size distribution in mass fraction, a result typically given by a common laboratory sieve

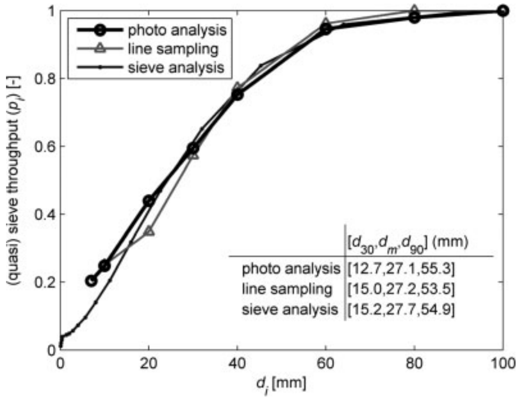

Figure 8. Typical grading curve for subsurface material resulting from Fig. 7 (see next page) in comparison with results from common analysis methods gained at same location.

analysis. The grain size distribution of the subsurface layer is approached via an empirical estimation of the percentage of non-detected finer grains. First comparisons of distributions obtained by automatic object detection, in-situ line sampling analysis and laboratory sieving indicate good agreement concerning the essential geometric parameters. The temporal effort for an analysis by automatic object detection is only at a fraction of the time needed for the standard methods. An additional benefit is that additional parameters are provided for each grain as well, namely the ratio of minor axis/major axis, the area, perimeter, center coordinates, and the grain orientation in the horizontal plane. These parameters are required to further analyze the characteristics of the bed material with respect to bed roughness, or armoring processes. Free access is given to the newly developed MATLAB-independent stand-alone tool based on the compiled code embedded in a GUI with pre-processing and post-processing options.

Currently the methodology is tested for their applicability to analyze subaqueous photographs taken in a dived, water-evacuated bell at the bed of river Rhine. A further purpose of this project is to measure river beds via images taken by divers or diving robotics. A successful proof would constitute an essential step in analyzing subaqueous granular beds.

Furthermore, derivatives of the above mentioned object detection techniques have been applied (a) to locate the water surface and bed from a side view image of a laboratory sectional model of a breaching dike (experimental setup: Schmocker & Hager, 2009), and (b) to identify and measure the diameter of an air entraining tube build by an intake vortex within PIV-images (experimental setup: Möller et. al, 2012). To sum up, techniques of automated object detection give an outstanding but unfortunately too rarely used tool for data acquisition, far beyond yielding at analyzing grain sizes.

ACKNOWLEDGEMENTS

The part-support by the Federal Office for the Environment (FOEN, Switzerland, 'Fluvial monitoring of the new Flaz River') and by the Federal Institute of Waterways (BAW, Germany, 'Expert monitoring and analysis of subaqueous digital images of river beds') is gratefully acknowledged.

REFERENCES

Buscombe, D., Rubin, D.M., Warrick, J.A. 2010. A universal approximation of grain size from images of non-cohesive sediment. *Journal of Geophysical Research*, 115(F02015).

Carbonneau, P.E., Lane, S.N., Bergeron, N.E. 2004. Catchment-scale mapping of surface grain size in gravel bed rivers using airborne digital imagery. *WRR* 40(W07202).

Fehr, R. 1987 . Einfache Bestimmung der Korngrössenverteilung von Geschiebematerial mit Hilfe der Linienzahlanalyse (Simple detection of grain size distribution of sediment material using line-count analysis). *Schweizer Ingenieur und Architekt* 105(38), 1104–1109 (in German).

Graham, D.J., Reid, I., Rice, S.P. 2005a. Automated sizing of coarse-grained sediments: Image-processing procedures. *Int. Association of Mathematical Geology* 37(1), 1–21.

Graham, D.J., Rice, S.P., Reid, I. 2005b. A transferable method for the automated grain sizing of river gravels, *Water Resources Research* 41(W07020).

Heritage, G.L., Milan, D.J. 2009. Terrestrial Laser scanning of grain roughness in a gravel-bed river. *Geomor.* 113, 4–11.

MATLAB, 2012. www.mathworks.com/help (2012/01/31).

Möller, G., Detert, M., Boes, R. 2012. Air entrainment due to vortices: State-of-the-art, Proc. 2nd*IAHR European Congress* Munich, Germany (in press).

Schmocker, L., Hager, W.H. (2009). Modelling dike breaching due to overtopping. *J. of Hydr. Research* 47(5), 585–597.

Weichert, R., Wickenhäuser, M., Bezzola, G.R., Minor, H.-E. 2004. Grain size analysis for coarse river beds using digital imagery processing. Proc. *RF* 2004, Naples, Italy, 753–760.

Wolman, M.G. 1954. A method of sampling coarse river-bed material. *Transactions American Geophysical Union* 35, 951–956.